Gravity-driven thin-film flow on a flexible substrate

P. D. Howell[1,†], **J. Robinson**[2] **and H. A. Stone**[3]

[1]Mathematical Institute, University of Oxford, 24–29 St Giles', Oxford OX1 3LB, UK

[2]Department of Mathematics, University of Bristol, University Walk, Bristol BS8 1TW, UK

[3]Department of Mechanical and Aerospace Engineering, Princeton University, Princeton, NJ 08544, USA

We study the flow of a thin liquid film along a flexible substrate. The flow is modelled using lubrication theory, assuming that gravity is the dominant driving force. The substrate is modelled as an elastic beam that deforms in two dimensions. Steady solutions are found using numerical and perturbation methods, and several different asymptotic regimes are identified. We obtain a complete characterization of how the length and stiffness of the beam and the imposed liquid flux determine the profile of the liquid film and the resulting beam deformation.

1. Introduction

Thin film flows are commonly studied in the Earth, engineering and materials sciences. The driving forces for flow can include buoyancy, surface tension and interfacial Marangoni stresses (Oron, Davis & Bankoff 1997; Craster & Matar 2009). Theoretical studies of thin liquid films often focus on flow over planar substrates. In the case of gravitational, or buoyant, driving of a flow over a horizontal base, the motion is driven by the slope of the free surface (Huppert 1982*b*), whereas for an inclined planar substrate the flow is principally driven by the component of gravity parallel to the substrate (Huppert 1982*a*). There have also been several investigations of flow of viscous thin films along rigid curved substrates, focusing on the influence of a given substrate curvature on capillary-driven flow (Jensen 1997; Myers, Charpin & Chapman 2002; Roy, Roberts & Simpson 2002; Howell 2003). In addition, there are studies of gravity-driven flows over specific fixed shapes (Duffy & Wilson 1999; Takagi & Huppert 2010).

However, there are physical situations where a liquid film flows over a compliant substrate, such that the substrate deformation and film flow are closely coupled. For example, surface-tension-driven flow of the liquid lining of the lungs has been considered by authors including Halpern & Grotberg (1992) and Heil & White (2002), while stability of thin-film flow over a compliant substrate has been studied by Matar, Craster & Kumar (2007) and Matar & Kumar (2007). In this paper we analyse a
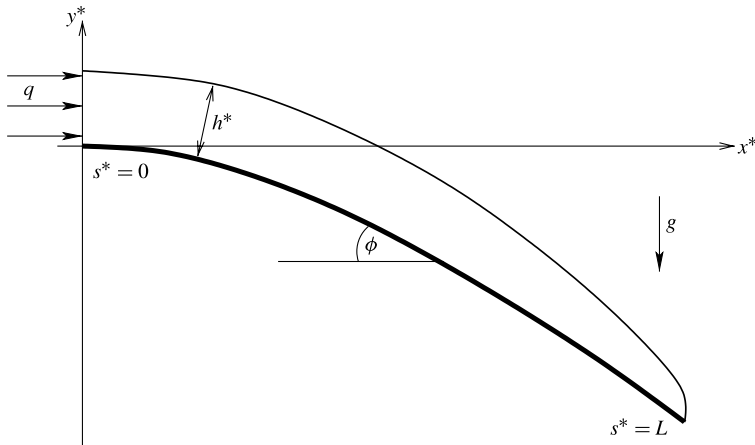
FIGURE 1. Schematic of a thin liquid film flowing along a flexible substrate.

model two-dimensional problem in which a thin liquid film causes large substrate deformations which in turn provide the principal driving force for the flow.

Our model set-up, illustrated in figure 1, is inspired by the example of rain water flowing over a leaf. We use the familiar lubrication approach for gravity-driven flow of a thin liquid film, where the hydrostatic pressure gradient depends both on the gradient of the film depth and on the local slope of the substrate. We assume that the substrate is a thin elastic beam whose shape is described by the Euler–Bernoulli model that couples the beam curvature to the tension and shear (transverse) forces imposed by the liquid film. We focus on steady flow due to a constant source at one end of the beam, which is clamped horizontally. The net result is a fifth-order system of ordinary differential equations, which we solve numerically and by asymptotic methods.

The problem description involves two dimensionless parameters: one (ε) measures the film thickness and the other (ℓ) represents the length of the substrate, both relative to a natural length scale that balances elastic and gravitational effects. The result of the asymptotic analysis is a complete characterization of the membrane shape and thin-film profile for $\varepsilon \ll 1$ for all possible values of ℓ.

In §2 we state and normalize the governing equations and boundary conditions. Then, in §3 we analyse the first of three distinguished limits identified, namely the 'small-deflection' regime, where the substrate deflection is comparable to the film height. In §4 we turn to the 'large-deflection' regime, where the substrate deflects by a distance comparable to its length and much greater than the film thickness. In this regime, the flow is driven principally by the tangential component of the gravitational body force. The various asymptotic approximations identified are summarized and combined in §5, and we draw our conclusions in §6.

2. Mathematical model

2.1. *Governing equations and boundary conditions*

The basic set-up is illustrated schematically in figure 1. We consider two-dimensional flow along a flexible substrate, parametrized by $x^* = x^*(s^*, t^*)$, $y^* = y^*(s^*, t^*)$, where s^* is arclength and t^* is time. We denote the downwards angle made by the substrate with

the horizontal by $\phi(s^*, t^*)$, so that

$$\frac{\partial x^*}{\partial s^*} = \cos\phi, \quad \frac{\partial y^*}{\partial s^*} = -\sin\phi. \tag{2.1}$$

For a thin film with negligible inertia, the film thickness $h^*(s^*, t^*)$ satisfies Reynolds' equation, namely

$$\frac{\partial h^*}{\partial t^*} = \frac{g}{3\nu}\frac{\partial}{\partial s^*}\left[h^{*3}\left(\cos\phi\frac{\partial h^*}{\partial s^*} - \sin\phi\right)\right], \tag{2.2}$$

where ν is the kinematic viscosity and g is the gravitational acceleration. The two bracketed terms on the right-hand side of (2.2) represent the transverse and tangential components of gravity, and we have assumed that surface tension is negligible.

The substrate is treated as an inextensible elastic beam bending under the normal and shear stresses exerted by the fluid, while the weight of the substrate itself is neglected by comparison. The tension T^* and shear force N^* thus satisfy the equations

$$\frac{\partial T^*}{\partial s^*} + N^*\frac{\partial\phi}{\partial s^*} = \rho g h^*\left(\cos\phi\frac{\partial h^*}{\partial s^*} - \sin\phi\right), \tag{2.3a}$$

$$\frac{\partial N^*}{\partial s^*} - T^*\frac{\partial\phi}{\partial s^*} = \rho g h^*\cos\phi, \tag{2.3b}$$

$$B\frac{\partial^2\phi}{\partial s^{*2}} = N^*, \tag{2.3c}$$

representing, respectively, tangential and transverse force balances and a balance of moments, where ρ is the density of the fluid and B is the bending stiffness of the beam.

We assume that the substrate is clamped horizontally at the origin, where a flux q of fluid is injected. Hence, we impose the boundary conditions

$$\phi = 0, \quad \frac{g h^{*3}}{3\nu}\frac{\partial h^*}{\partial s^*} = -q \quad \text{at } s^* = 0. \tag{2.4}$$

We denote the length of the substrate by L. The end $s^* = L$ is assumed to be free, with no applied forces or moments, so that

$$T^* = N^* = \frac{\partial\phi}{\partial s^*} = 0 \quad \text{at } s^* = L. \tag{2.5}$$

If the substrate is initially dry, then a thin film will spread from the source at $s^* = 0$, eventually covering the entire substrate. Thereafter, we assume that the film falls directly from the end of the beam, i.e. that $h^*(L, t^*) = 0$. Although the film thickness is assumed to be zero, there will still be a non-zero flux of liquid flowing over the end of the beam. When the film has reached a steady state, this flux from the end must exactly balance the flux q injected at $s^* = 0$, so that

$$h^* = 0, \quad \frac{g h^{*3}}{3\nu}\frac{\partial h^*}{\partial s^*} = -q \quad \text{at } s^* = L. \tag{2.6}$$

These conditions imply weakly singular local behaviour with $h^* \sim (12\nu q(L - s^*)/g)^{1/4}$ as $s^* \to L$. Presumably there is an inner problem near $s^* = L$ where other physical effects become important, for example surface tension and two-dimensionality, and we are effectively assuming that (2.6) are the effective boundary conditions that would

result from matching with such a region. An analogous boundary condition of zero film height has been employed in previous studies of gravity currents on horizontal substrates, for example Boussinesq (1904), Rupp & Selker (2005) and Zheng *et al.* (2013). The applicability of this boundary condition when the substrate is significantly deflected from the horizontal will be discussed below.

2.2. *Non-dimensionalization*

It is useful to non-dimensionalize the steady-state equations using the intrinsic length scale

$$a = \left(\frac{B}{\rho g} \right)^{1/4}, \tag{2.7}$$

rather than the plate length L. The variables are then scaled as follows:

$$s^* = as, \quad h^* = \varepsilon ah, \quad \phi = \varepsilon \psi, \tag{2.8a}$$

$$T^* = \varepsilon^2 \rho g a^2 T, \quad N^* = \varepsilon \rho g a^2 N, \tag{2.8b}$$

where

$$\varepsilon = \left(\frac{3\nu q}{g a^3} \right)^{1/4}. \tag{2.9}$$

The dimensionless steady governing equations are

$$h^3 \left(\cos(\varepsilon \psi) \frac{\mathrm{d}h}{\mathrm{d}s} - \frac{\sin(\varepsilon \psi)}{\varepsilon} \right) = -1, \tag{2.10a}$$

$$\frac{\mathrm{d}T}{\mathrm{d}s} + N \frac{\mathrm{d}\psi}{\mathrm{d}s} = h \left(\cos(\varepsilon \psi) \frac{\mathrm{d}h}{\mathrm{d}s} - \frac{\sin(\varepsilon \psi)}{\varepsilon} \right), \tag{2.10b}$$

$$\frac{\mathrm{d}N}{\mathrm{d}s} - \varepsilon^2 T \frac{\mathrm{d}\psi}{\mathrm{d}s} = h \cos(\varepsilon \psi), \tag{2.10c}$$

$$\frac{\mathrm{d}^2 \psi}{\mathrm{d}s^2} = N, \tag{2.10d}$$

while the boundary conditions are

$$\psi = 0 \quad \text{at } s = 0, \tag{2.10e}$$

$$h = T = N = \frac{\mathrm{d}\psi}{\mathrm{d}s} = 0 \quad \text{at } s = \ell, \tag{2.10f}$$

where

$$\ell = \frac{L}{a} \tag{2.11}$$

is the dimensionless beam length.

3. Small-deflection regime

3.1. *Leading-order equations*

The problem involves two dimensionless parameters: ε and ℓ. We assume that $\varepsilon \ll 1$, implying that the film is thin compared with the characteristic length scale a for beam deformation. In scaling ϕ with ε in (2.8a), we are considering a distinguished limit

where the lateral deflection of the beam is comparable to the film thickness. This limit will occur if the beam is relatively short, specifically if $\ell = O(1)$. In this regime, the tangential and transverse components of gravity in (2.2) and (2.3*a*) balance. In § 4, we will consider an alternative distinguished limit that applies for longer beams where $\phi = O(1)$ and large beam deflections are possible.

To facilitate numerical solution, it is helpful to define

$$z = \ell - s. \tag{3.1}$$

Then taking $\varepsilon \to 0$ in (2.10), we obtain the leading-order equations

$$\frac{\mathrm{d}h}{\mathrm{d}z} = \frac{1}{h^3} - \psi, \qquad \frac{\mathrm{d}^3\psi}{\mathrm{d}z^3} = -h, \tag{3.2}$$

with errors of $O(\varepsilon^2)$. In this reduced model, the beam undergoes purely transverse bending under the weight of the liquid film, while the flow is driven by both tangential and transverse components of gravity. The corresponding boundary conditions are

$$h = \frac{\mathrm{d}\psi}{\mathrm{d}z} = \frac{\mathrm{d}^2\psi}{\mathrm{d}z^2} = 0, \quad \psi = \Psi \quad \text{at } z = 0, \tag{3.3a}$$

$$\psi = 0 \quad \text{at } z = \ell, \tag{3.3b}$$

where we have introduced $\Psi = \psi|_{s=\ell} = \varepsilon^{-1}\phi|_{s=\ell}$. This variable represents the (unknown) scaled rotation of the free end of the beam, which will be used as a net measure of the deflection.

For each value of Ψ, equation (3.2) has a unique solution satisfying the initial conditions (3.3*a*), with asymptotic behaviour

$$h \sim \sqrt{2}z^{1/4} - \frac{4\Psi}{7}z + \frac{24\sqrt{2}\Psi^2}{245}z^{7/4} + \frac{64\Psi^3}{3185}z^{5/2} + \cdots, \quad \psi \sim \Psi - \frac{64\sqrt{2}}{585}z^{13/4} + \cdots \tag{3.4}$$

as $z \to 0$ (or $s \to \ell$). We solve this initial-value problem numerically for each value of Ψ and read off the corresponding value of ℓ from the condition (3.3*b*). The result of this procedure is plotted in figure 2, which shows that there is a monotonic one-to-one relationship between the end deflection Ψ and the dimensionless beam length ℓ.

An additional characteristic of the flow is provided in figure 3, where we plot the dimensionless film thickness at the origin, $h_0 = h|_{s=0}$, versus the dimensionless beam length ℓ. Not surprisingly, the film height tends to zero as the beam length tends to zero. However, h_0 takes a maximum value ≈ 1.3718 when $\ell \approx 1.1643$, before then decreasing again as ℓ tends to infinity. As the length of the beam increases, its downwards deflection increases and the component of gravitational acceleration along the beam therefore also increases. Hence, fluid is transported away from the origin at an enhanced rate and, thus, the film height eventually starts to decrease.

In figure 4 we plot the beam deflection and the film height obtained by solving (3.2)–(3.3) numerically, for different values of $\ell = 0.5, 1, 2, 4$. In the small-deflection regime, the leading-order beam and film profiles are given by

$$y(x) = \varepsilon \int_0^x \psi(s)\,\mathrm{d}s \quad \text{and} \quad y(x) = \varepsilon \int_0^x \psi(s)\,\mathrm{d}s + \varepsilon h(x), \tag{3.5}$$

respectively. As ℓ increases from 0.5 to 1, the film thickness increases while also exhibiting the expected 1/4-root singularity at the edge of the substrate $x = \ell$. However, further increase in ℓ gives rise to significantly larger beam deflections, which
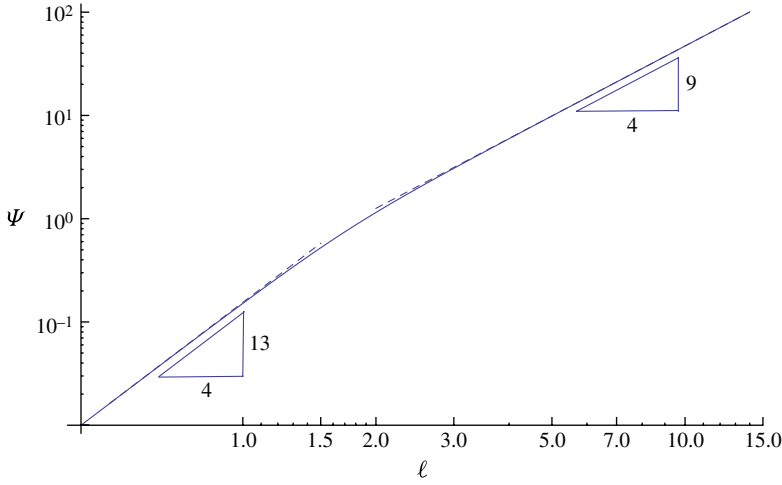
FIGURE 2. (Colour online) The scaled rotation Ψ of the free end of the beam plotted versus dimensionless beam length ℓ using logarithmic axes. The dashed curves show the asymptotic limits (3.9) as $\ell \to 0$ and (3.15) as $\ell \to \infty$.
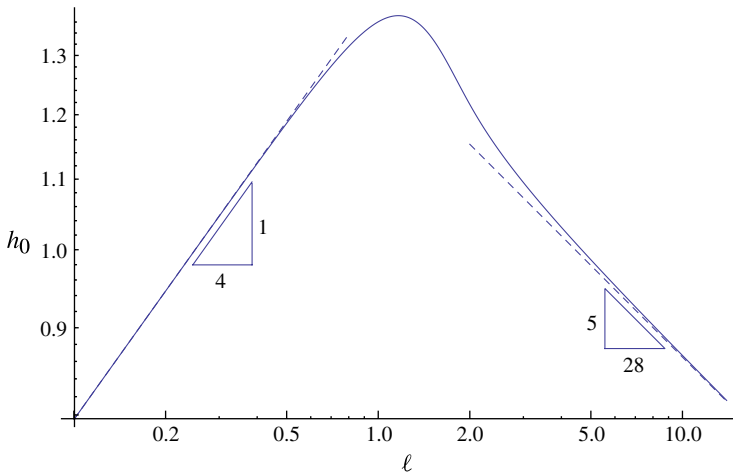

FIGURE 3. (Colour online) The dimensionless film height h_0 at the origin plotted versus dimensionless beam length ℓ using logarithmic axes. The dashed curves show the asymptotic limits (3.10) as $\ell \to 0$ and (3.28) as $\ell \to \infty$.

in turn lead to a decrease in the film thickness. As ℓ becomes larger still, a boundary layer at the free edge $x = \ell$ becomes evident, and a boundary layer at the origin also starts to form, with the film thickening noticeably close to $x = 0$.

To understand the behaviours observed in figures 2–4, we will next explore the asymptotic behaviour of the system (3.2)–(3.3b) as $\Psi \to 0$ (small deflections) and as $\Psi \to \infty$ (large deflections).
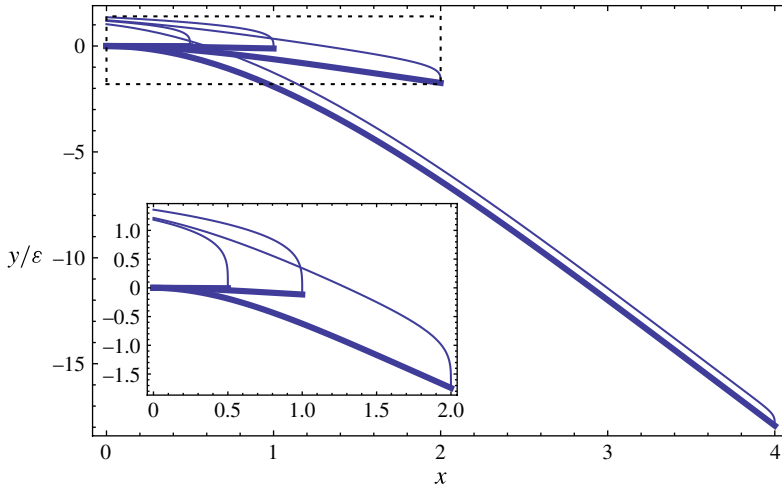
FIGURE 4. (Colour online) The beam deflection and film profile given by the problem (3.2)–(3.3) plotted in the $(x, y/\varepsilon)$-plane for $\ell = 0.5, 1, 2, 4$. The inset focuses on the cases where $\ell = 0.5, 1, 2$.

3.2. *Small-Ψ limit*

For small Ψ, we perform the rescaling

$$\psi = \Psi \psi', \quad h = \Psi^{1/13} h', \quad z = \Psi^{4/13} z', \tag{3.6}$$

before letting $\Psi \to 0$ to obtain the leading-order equations

$$\frac{\mathrm{d}h'}{\mathrm{d}z'} = \frac{1}{h'^3}, \quad \frac{\mathrm{d}^3\psi'}{\mathrm{d}z'^3} = -h'. \tag{3.7}$$

Here the film profile $h'(z')$ behaves as if the beam were completely flat, and the small transverse displacement is determined *a posteriori*. After applying the initial conditions (3.3a), we find the leading-order solutions

$$h' = \sqrt{2}\, z'^{1/4}, \quad \psi' = 1 - \frac{64\sqrt{2}}{585} z'^{13/4}. \tag{3.8}$$

Hence, $\psi' = 0$ at $z' = \left(585/64\sqrt{2}\right)^{4/13}$, and we infer that the free-end rotation is given by

$$\Psi \sim \frac{64\sqrt{2}}{585} \ell^{13/4} \quad \text{as } \ell \to 0. \tag{3.9}$$

This result is plotted as a dashed curve in figure 2.

We also obtain the film height at the origin by evaluating h' when $\psi' = 0$, which leads to the result

$$h_0 \sim \sqrt{2}\, \ell^{1/4} \quad \text{as } \ell \to 0. \tag{3.10}$$

This is the film height expected for a fixed horizontal substrate of length ℓ, since the beam becomes effectively rigid as its length tends to zero. As shown by a dashed curve in figure 3, the numerical results agree well with (3.10) for $\ell \lesssim 0.5$.
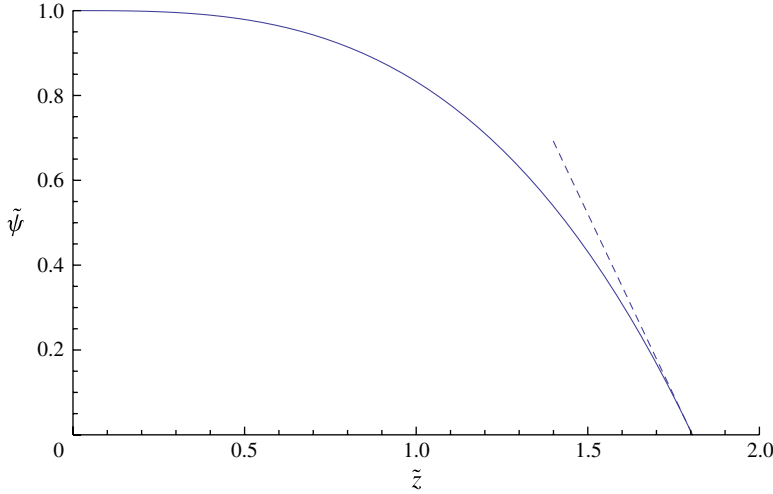
FIGURE 5. (Colour online) The function $\tilde{\psi}(\tilde{z})$ satisfying the problem (3.13). The asymptotic behaviour (3.20) is shown as a dashed curve.

3.3. *Large-Ψ limit*

At the other limit where $\Psi \to \infty$, we return to the problem (3.2), (3.3) and perform the rescaling

$$\psi = \Psi \tilde{\psi}, \quad z = \Psi^{4/9} \tilde{z}, \quad h = \Psi^{-1/3} \tilde{h}, \tag{3.11}$$

to obtain the system

$$\Psi^{-16/9} \frac{d\tilde{h}}{d\tilde{z}} = \frac{1}{\tilde{h}^3} - \tilde{\psi}, \quad \frac{d^3 \tilde{\psi}}{d\tilde{z}^3} = -\tilde{h}. \tag{3.12}$$

For large beam deflection, the tangential component of gravity becomes dominant, and the film thickness depends only on the slope of the substrate: $\tilde{h} = \tilde{\psi}^{-1/3}$ to leading order as $\Psi \to \infty$. Hence, $\tilde{\psi}$ satisfies the nonlinear third-order differential equation

$$\tilde{\psi}^{1/3} \frac{d^3 \tilde{\psi}}{d\tilde{z}^3} = -1, \tag{3.13a}$$

and the initial conditions

$$\tilde{\psi} = 1, \quad \frac{d\tilde{\psi}}{d\tilde{z}} = \frac{d^2 \tilde{\psi}}{d\tilde{z}^2} = 0 \quad \text{at } \tilde{z} = 0. \tag{3.13b}$$

A numerical solution of the problem (3.13) is plotted in figure 5. We find numerically that $\tilde{\psi} \to 0$ at a finite value of $\tilde{z}$, namely

$$\tilde{z} = \tilde{\ell} \approx 1.804915. \tag{3.14}$$

By reversing the scaling (3.11), we infer that $\Psi \sim \left(\ell/\tilde{\ell} \right)^{9/4}$, that is,

$$\Psi \sim 0.2648 \, \ell^{9/4} \quad \text{as } \ell \to \infty. \tag{3.15}$$

As indicated by a dashed curve in figure 2, this result agrees well with our numerical solution.

However, this leading-order solution fails to satisfy the boundary condition $\tilde{h} = 0$ at $\tilde{z} = 0$ (i.e. at the free end of the beam). This observation is explained by the existence of a boundary layer, where $\tilde{h}$ adjusts to the imposed value of 0 over an increasingly narrow region as Ψ increases. The film thickness $\tilde{h} = \tilde{\psi}^{-1/3}$ also appears to tend to infinity as $\tilde{\psi} \to 0$ (i.e. at the clamped end). This occurs because the assumption that the tangential component of gravity is dominant ceases to apply when $\tilde{\psi}$ is sufficiently small, and is resolved by examining a boundary layer at $\tilde{z} = \ell$ where the transverse component of gravity regains its importance.

First considering the boundary layer at the free end $\tilde{z} = 0$, we let

$$\tilde{z} = \Psi^{-16/9}\bar{z}, \tag{3.16}$$

which results in the leading-order inner equations

$$\frac{\mathrm{d}\tilde{h}}{\mathrm{d}\bar{z}} = \frac{1}{\tilde{h}^3} - \tilde{\psi}, \quad \frac{\mathrm{d}^3\tilde{\psi}}{\mathrm{d}\bar{z}^3} = 0, \tag{3.17}$$

and the matching conditions $\tilde{h} \to 1$, $\tilde{\psi} \to 1$ as $\bar{z} \to \infty$. We therefore have $\tilde{\psi} \equiv 1$ to leading order, and the film height in this boundary layer satisfies the differential equation

$$\frac{\mathrm{d}\tilde{h}}{\mathrm{d}\bar{z}} = \frac{1}{\tilde{h}^3} - 1. \tag{3.18}$$

The solution satisfying the boundary condition $\tilde{h} = 0$ at $\bar{z} = 0$ is given by the implicit equation

$$\bar{z} = \frac{1}{6} \log \left(\frac{1 + \tilde{h} + \tilde{h}^2}{\left(1 - \tilde{h}\right)^2} \right) - \tilde{h} + \frac{1}{\sqrt{3}} \tan^{-1} \left(\frac{\sqrt{3}\,\tilde{h}}{2 + \tilde{h}} \right). \tag{3.19}$$

As pointed out above, the outer solution plotted in figure 5 also appears to imply that $\tilde{h} \to \infty$ as $\tilde{z} \to \tilde{\ell}$, and there is yet another boundary layer in which this growth is cut off. To assist with matching, which will establish the film height h_0 at the origin, we note that

$$\tilde{\psi} \sim A_0 \left(\tilde{\ell} - \tilde{z} \right) \quad \text{as } \tilde{z} \to \tilde{\ell}, \tag{3.20}$$

as illustrated in figure 5, where

$$A_0 \approx 1.70799 \tag{3.21}$$

is determined numerically. Thus, following the further rescaling

$$\tilde{z} = \tilde{\ell} - A_0^{-4/7} \Psi^{-16/21} \hat{z}, \quad \tilde{\psi} = A_0^{3/7} \Psi^{-16/21} \hat{\psi}, \quad \tilde{h} = A_0^{-1/7} \Psi^{16/63} \hat{h}, \tag{3.22}$$

we obtain the leading-order equations

$$\frac{\mathrm{d}\hat{h}}{\mathrm{d}\hat{z}} = \hat{\psi} - \frac{1}{\hat{h}^3}, \quad \frac{\mathrm{d}^3\hat{\psi}}{\mathrm{d}\hat{z}^3} = 0, \tag{3.23}$$

as $\Psi \to \infty$, subject to the matching conditions

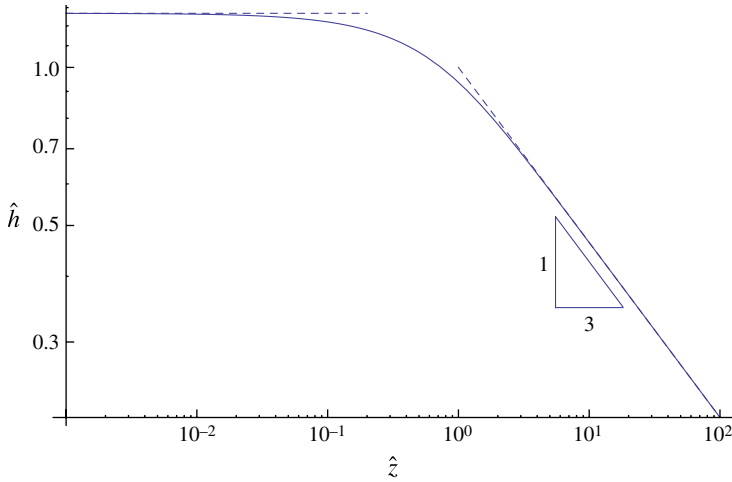$$\hat{h} \sim \hat{z}^{-1/3}, \quad \hat{\psi} \sim \hat{z} \quad \text{as } \hat{z} \to \infty. \tag{3.24}$$

FIGURE 6. (Colour online) The solution $\hat{h}\left(\hat{z}\right)$ to the differential equation (3.25) and the matching condition (3.24), plotted using logarithmic axes. The limiting behaviours (3.26) as $\hat{z} \to 0$ and (3.24) as $\hat{z} \to \infty$ are plotted as dashed curves.

Hence, $\hat{\psi} \equiv \hat{z}$ and $\hat{h}$ satisfies the equation

$$\frac{\mathrm{d}\hat{h}}{\mathrm{d}\hat{z}} = \hat{z} - \frac{1}{\hat{h}^3}, \tag{3.25}$$

and the matching condition (3.24). A numerical solution of this problem is plotted in figure 6. We discover numerically that the solution satisfies

$$\hat{h} \to B_0 \approx 1.26772 \quad \text{as } \hat{z} \to 0, \tag{3.26}$$

and we deduce that the film thickness at the origin is given asymptotically by

$$h_0 \sim B_0 A_0^{-1/7} \Psi^{-5/63} \quad \text{as } \Psi \to \infty. \tag{3.27}$$

Using the relation (3.15), we therefore obtain

$$h_0 \sim 1.30499 \, \ell^{-5/28} \quad \text{as } \ell \to \infty. \tag{3.28}$$

This result is plotted as a dashed curve in figure 3, which confirms that (3.28) agrees with our numerical solution.

4. Large-deflection regime

4.1. *Distinguished limit*

The above analysis of small deflections suggests that the plate may undergo an unbounded deflection as $\ell \to \infty$. However, if ℓ is sufficiently large, a new distinguished limit emerges in which the plate suffers an $O(1)$ deflection. To examine this regime, we return to (2.10) and rescale the variables as follows:

$$s = \varepsilon^{-4/9} S, \quad h = \varepsilon^{1/3} H, \quad T = \varepsilon^{-10/9} \mathscr{T}, \quad N = \varepsilon^{-1/9} \mathscr{N}, \tag{4.1}$$

where ε is again defined by (2.9). The problem is thus transformed to

$$H^3 \left(\delta \cos\phi \frac{dH}{dS} - \sin\phi \right) = -1, \tag{4.2a}$$

$$\frac{d\mathscr{T}}{dS} + \mathscr{N} \frac{d\phi}{dS} = H \left(\delta \cos\phi \frac{dH}{dS} - \sin\phi \right), \tag{4.2b}$$

$$\frac{d\mathscr{N}}{dS} - \mathscr{T} \frac{d\phi}{dS} = H \cos\phi, \tag{4.2c}$$

$$\frac{d^2\phi}{dS^2} = \mathscr{N}, \tag{4.2d}$$

with boundary conditions

$$\phi = 0 \quad \text{at } S = 0, \tag{4.2e}$$

$$H = \mathscr{T} = \mathscr{N} = \frac{d\phi}{dS} = 0 \quad \text{at } S = \lambda, \tag{4.2f}$$

where we introduce the shorthand

$$\delta = \varepsilon^{16/9} = \left(\frac{3\nu q}{ga^3} \right)^{4/9} \quad \text{and} \quad \lambda = \varepsilon^{4/9}\ell = \frac{\varepsilon^{4/9}L}{a}. \tag{4.3}$$

4.2. *Leading-order equations*

As $\delta \to 0$, (4.2a) implies that

$$H = \frac{1}{\sin^{1/3}\phi}. \tag{4.4}$$

As is standard for gravity-driven thin-film flow on a curved surface, the transverse component of gravity is subdominant and the leading-order film thickness is determined purely in terms of the local substrate inclination (as in, for example, Duffy & Wilson 1999). We anticipate that there will be a boundary layer at $S = 0$ to prevent H from tending to infinity and a second boundary layer at the free end $S = \lambda$, so that the imposed boundary condition $H(\lambda) = 0$ may be satisfied.

Equations (4.2b) and (4.2c) thus reduce to

$$\frac{d\mathscr{T}}{dS} + \mathscr{N} \frac{d\phi}{dS} = -\sin^{2/3}\phi, \tag{4.5a}$$

$$\frac{d\mathscr{N}}{dS} - \mathscr{T} \frac{d\phi}{dS} = \frac{\cos\phi}{\sin^{1/3}\phi}, \tag{4.5b}$$

which may be combined to give

$$\frac{d}{dS} \left(\mathscr{T} \cos\phi + \mathscr{N} \sin\phi \right) = 0, \tag{4.6}$$

which represents a horizontal force balance. From the boundary conditions (4.2f) we deduce that the bracketed term in (4.6) is identically zero and, hence, that

$$\mathscr{T} = F \sin\phi, \quad \mathscr{N} = -F \cos\phi, \tag{4.7}$$

for some function $F(S)$, representing the vertical stress component in the beam. Equations (4.2b)–(4.2d) thus reduce to the system

$$\frac{\mathrm{d}F}{\mathrm{d}S} = -\sin^{-1/3}\phi, \quad \frac{\mathrm{d}^2\phi}{\mathrm{d}S^2} = -F\cos\phi, \tag{4.8}$$

subject to the boundary conditions

$$\phi(0) = 0, \quad \frac{\mathrm{d}\phi}{\mathrm{d}S}(\lambda) = 0, \quad F(\lambda) = 0. \tag{4.9}$$

To facilitate numerical solution, we introduce the beam curvature

$$\kappa = \frac{\mathrm{d}\phi}{\mathrm{d}S} \tag{4.10}$$

and rewrite the system (4.8) in the form

$$\frac{\mathrm{d}F}{\mathrm{d}\phi} = -\frac{1}{\kappa\sin^{1/3}\phi}, \quad \frac{\mathrm{d}\kappa}{\mathrm{d}\phi} = -\frac{F\cos\phi}{\kappa}. \tag{4.11}$$

We shoot from $\phi = \Phi$, using the local behaviour

$$F \sim \frac{6^{1/3}(\Phi-\phi)^{1/3}}{\cos^{1/3}\Phi\sin^{2/9}\Phi}\left\{1 + \frac{7\cot\Phi - 6\tan\Phi}{90}(\Phi-\phi)\right.$$
$$\left. + \frac{54\sec^2\Phi + 97\csc^2\Phi - 79}{3240}(\Phi-\phi)^2 + \cdots\right\}, \tag{4.12a}$$

$$\kappa \sim \frac{3^{2/3}\cos^{1/3}\Phi(\Phi-\phi)^{2/3}}{2^{1/3}\sin^{1/9}\Phi}\left\{1 + \frac{\cot\Phi + 12\tan\Phi}{45}(\Phi-\phi)\right.$$
$$\left. + \frac{31\csc^2\Phi - 246\sec^2\Phi - 246}{5400}(\Phi-\phi)^2 + \cdots\right\} \tag{4.12b}$$

as $\phi \to \Phi$, integrate to $\phi = 0$, then read off the corresponding values of $\kappa(0) = A$, say, and

$$\lambda = \int_0^\Phi \frac{\mathrm{d}\phi}{\kappa(\phi)}. \tag{4.13}$$

By following this procedure, we can back out the dependence of Φ and A on the dimensionless beam length λ, and the resulting functions are plotted in figures 7 and 8, respectively. The dashed curves show the small- and large-λ asymptotic limits, which will be derived below. We note that the local expansions (4.12) are evidently non-uniform if Φ is very close to $\pi/2$, and we return to this limit in §4.6.

In figure 9, we show typical profiles of the beam and the film obtained by solving (4.11) and (4.12) numerically with dimensionless beam length $\lambda = 1, 2, 3$. In plotting the film thickness, given by (4.4), we use a value $\varepsilon = 0.05$ for the aspect ratio. We see that, as expected, a longer beam suffers a greater deflection and carries a thinner film. It is evident that this outer solution predicts an unbounded film thickness at the origin, and this is resolved below by analysing a boundary layer at $S = 0$. It is also clear that the assumed condition of zero film thickness at the free end $S = \lambda$ is not satisfied. This boundary condition is not strictly appropriate when the beam is no longer approximately horizontal, and anyway the leading-order outer solution is independent of the boundary condition applied for H. Nevertheless, for completeness
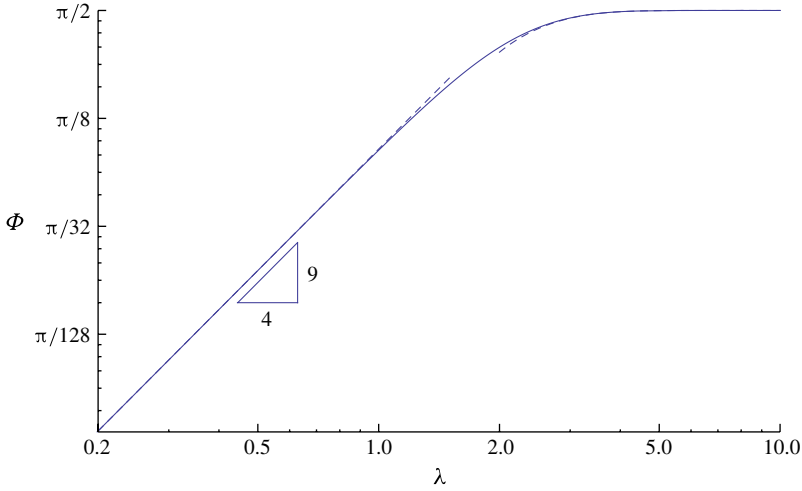
FIGURE 7. (Colour online) Deflection angle Φ plotted versus dimensionless beam length λ using logarithmic axes. The dashed curves show the asymptotic limits (4.24*a*) as $\lambda \to 0$ and (4.32) as $\lambda \to \infty$. (The tick marks on the vertical axis are at $\Phi = n\pi/4^m$, where $n \in \{3, 4, 5, 6, 7, 8\}$ and $m \in \{2, 3, 4\}$.)
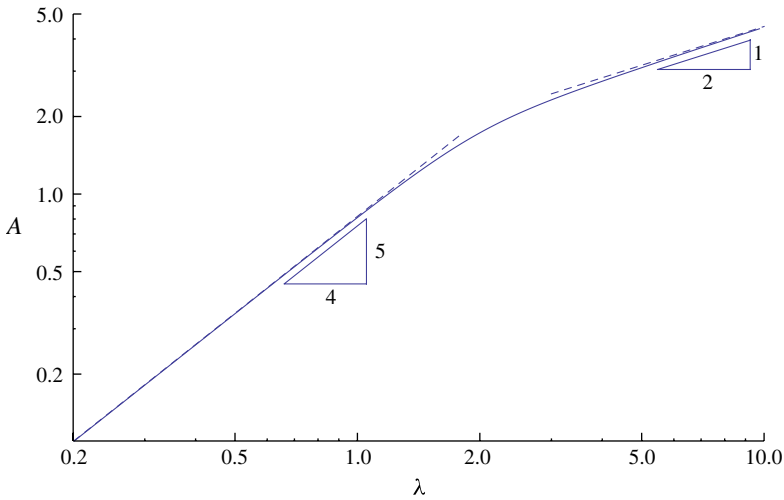

FIGURE 8. (Colour online) Beam curvature at the origin $A = \kappa(0)$ plotted versus dimensionless beam length λ using logarithmic axes. The dashed curves show the asymptotic limits (4.24*b*) as $\lambda \to 0$ and (4.33) as $\lambda \to \infty$.

we will also demonstrate that it is possible to specify $H(\lambda) = 0$ by considering a boundary layer at $S = \lambda$.

4.3. *Boundary layers*

As in § 3.3, the tangential component of gravity dominates the flow in the body of the film where the beam deflection is large. However, at the clamped end $S = 0$ where $\phi = 0$, this is no longer the case, and a balance between the tangential and transverse
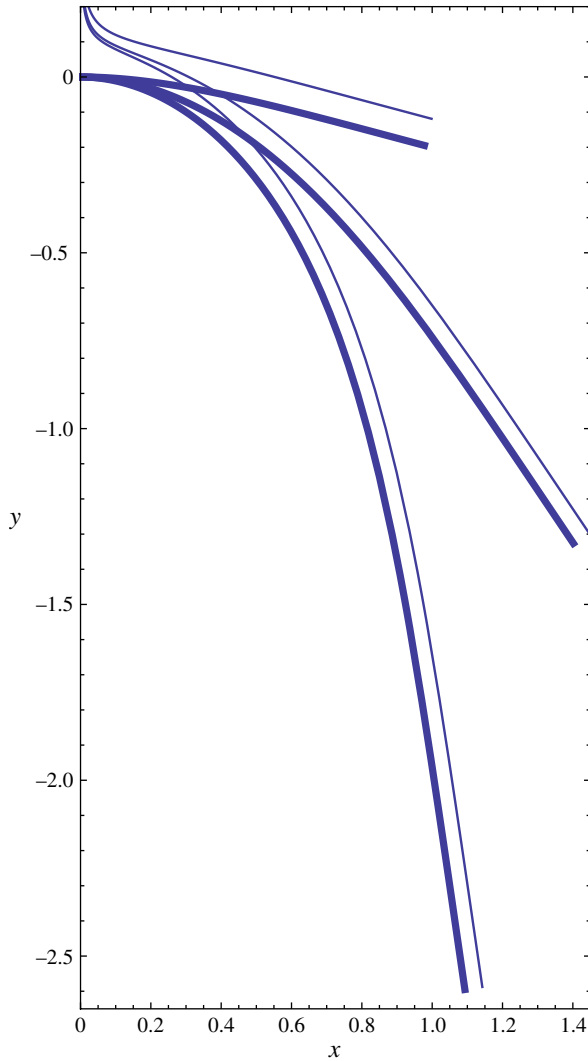
FIGURE 9. (Colour online) The beam deflection and film profile obtained by numerical solution of (4.11)–(4.12) plotted in the (x, y)-plane with $\varepsilon = 0.05$ and $\lambda = 1, 2, 3$.

components of gravity is obtained through the rescalings

$$
\left.
\begin{aligned}
S &= A^{-1}(\delta A)^{3/7}\hat{z}, \quad H = (\delta A)^{-1/7}\hat{h}, \quad \phi = (\delta A)^{3/7}\hat{\psi}, \\
\mathscr{T} &= (\delta A)^{3/7}\hat{\mathscr{T}}, \quad \mathscr{N} = \hat{\mathscr{N}}
\end{aligned}
\right\}
\tag{4.14}
$$

which results in the leading-order equations

$$
\frac{\mathrm{d}\hat{h}}{\mathrm{d}\hat{z}} = \hat{\psi} - \frac{1}{\hat{h}^3}, \quad \frac{\mathrm{d}\hat{\mathscr{T}}}{\mathrm{d}\hat{z}} + \hat{\mathscr{N}}\frac{\mathrm{d}\hat{\psi}}{\mathrm{d}\hat{z}} = 0, \quad \frac{\mathrm{d}\hat{\mathscr{N}}}{\mathrm{d}\hat{z}} = 0, \quad \frac{\mathrm{d}^2\hat{\psi}}{\mathrm{d}\hat{z}^2} = 0,
\tag{4.15}
$$

with corrections of order $\delta^{2/7}$. These equations are to be solved subject to the boundary condition $\hat{\psi}(0) = 0$ and the matching conditions

$$\hat{h} \sim \hat{z}^{-1/3}, \quad \hat{\psi} \sim \hat{z}, \quad \hat{\mathscr{T}} \sim F_0 \hat{z}, \quad \mathscr{N} \sim -F_0 \quad \text{as } \hat{z} \to \infty, \tag{4.16}$$

where $F_0 = F(0)$. Hence, to leading order we have

$$\hat{\psi} = \hat{z}, \quad \hat{\mathscr{T}} = F_0 \hat{z}, \quad \mathscr{N} = -F_0, \tag{4.17}$$

and the film thickness in the boundary layer satisfies the problem

$$\frac{\mathrm{d}\hat{h}}{\mathrm{d}\hat{z}} = \hat{z} - \frac{1}{\hat{h}^3}, \quad \hat{h} \sim \hat{z}^{-1/3} \quad \text{as } \hat{z} \to \infty. \tag{4.18}$$

This is identical to the problem (3.24), (3.25) solved above, and we can read off the value $\hat{h}(0) = B_0 \approx 1.26772$. Hence, the scaled film thickness at the origin is given by

$$H(0) \sim B_0 (\delta A)^{-1/7}, \tag{4.19}$$

where A is given in terms of the dimensionless beam length λ by the function plotted in figure 8.

The boundary layer at the free end $S = \lambda$ and $\phi = \Phi$ is analysed by performing the rescalings:

$$S = \lambda - \frac{\delta \cos \Phi}{\sin^{4/3} \Phi} \bar{z}, \quad H = \frac{\hat{h}}{\sin^{1/3} \Phi}, \quad \phi = \Phi + \frac{\delta^3 \cos^3 \Phi}{\sin^{11/3} \Phi} \hat{\phi}, \tag{4.20}$$

$$\mathscr{T} = \frac{\delta \cos \Phi}{\sin^{2/3} \Phi} \hat{\mathscr{T}}, \quad \mathscr{N} = \frac{\delta \cos \Phi}{\sin^{5/3} \Phi} \hat{\mathscr{N}}. \tag{4.21}$$

At leading order, we then find that $\hat{h}(\bar{z})$ satisfies the initial-value problem

$$\frac{\mathrm{d}\hat{h}}{\mathrm{d}\bar{z}} = \frac{1}{\hat{h}^3} - 1, \quad \hat{h}(0) = 0. \tag{4.22}$$

Again, we have encountered this problem before, and the solution is given by the implicit (3.19); then $\hat{\phi}$, $\hat{\mathscr{T}}$ and $\hat{\mathscr{N}}$ may be determined *a posteriori* from decoupled differential equations.

4.4. *Small-λ limit*

When the scaled beam length λ is small, the deflection angle Φ is also small, and the scalings

$$S = \lambda - \Phi^{4/9} \tilde{z}, \quad \phi = \Phi \tilde{\psi} \tag{4.23}$$

transform the outer problem (4.8) into the problem (3.13) found previously for $\tilde{\psi}(\tilde{z})$. This confirms that the small- and large-deflection solutions match for intermediate values of Φ and λ. We can thus infer the small-λ asymptotic limits of the present large-deflection solutions, namely

$$\Phi \sim \left(\frac{\lambda}{\bar{\ell}}\right)^{9/4} \approx 0.264833 \, \lambda^{9/4}, \tag{4.24a}$$

$$A \sim A_0 \left(\frac{\lambda}{\bar{\ell}}\right)^{5/4} \approx 0.816422 \, \lambda^{5/4} \tag{4.24b}$$

as $\lambda \to 0$. The dashed curves in figures 7 and 8 demonstrate the accuracy of these estimates.

4.5. *Large-λ limit*

Next we consider the opposite extreme where the scaled beam length $\lambda \to \infty$. In this limit, the beam sags until it is almost vertical, so that $\Phi \to \pi/2$, and gravity causes the vertical stress F to scale with the beam length λ. We therefore perform the scalings

$$S = \lambda\zeta, \quad \phi = \frac{\pi}{2} - \chi, \quad F = \lambda f, \tag{4.25}$$

and it transpires that χ is exponentially small, so that the film thickness H is approximately uniform (and equal to 1), as would be expected for flow down a vertical substrate. The model (4.8) is therefore transformed into

$$\frac{\mathrm{d}f}{\mathrm{d}\zeta} = -1 \quad \frac{1}{\lambda^3}\frac{\mathrm{d}^2\chi}{\mathrm{d}\zeta^2} = f\chi, \tag{4.26}$$

to lowest order, with boundary conditions

$$f = \frac{\mathrm{d}\chi}{\mathrm{d}\zeta} = 0 \quad \text{at } \zeta = 1. \tag{4.27}$$

The leading-order solutions are therefore

$$f(\zeta) = 1 - \zeta, \quad \chi(\zeta) = \frac{3^{1/6}\Gamma(2/3)C}{2}\left\{\sqrt{3}\mathrm{Ai}\big(\lambda(1-\zeta)\big) + \mathrm{Bi}\big(\lambda(1-\zeta)\big)\right\}, \tag{4.28}$$

where $C = \chi(1)$ is an integration constant and Ai, Bi denote Airy functions.

This solution must match with an inner region near $\zeta = 0$ where ϕ adjusts from $\pi/2$ to 0. To analyse this region, we return to the system (4.8) and perform the rescaling

$$\zeta = \lambda^{-3/2}\xi \quad \text{that is, } S = \lambda^{-1/2}\xi, \tag{4.29}$$

to get the leading-order inner equations

$$\frac{\mathrm{d}f}{\mathrm{d}\xi} = 0, \quad \frac{\mathrm{d}^2\phi}{\mathrm{d}\xi^2} = -f\cos\phi. \tag{4.30}$$

By applying the boundary condition $\phi(0) = 0$ and matching with (4.28), we deduce that $f = 1$ and

$$\phi = \frac{\pi}{2} - 4\tan^{-1}\left(\left(\sqrt{2}-1\right)\mathrm{e}^{-\xi}\right) \tag{4.31}$$

in the inner region. Finally, by matching the inner and outer solutions for ϕ, we evaluate the integration constant C and, hence, deduce the asymptotic behaviour

$$\Phi \sim \frac{\pi}{2} - \frac{8\left(\sqrt{2}-1\right)\sqrt{\pi}}{3^{1/6}\Gamma(2/3)}\lambda^{1/4}\mathrm{e}^{-2\lambda^{3/2}/3} \quad \text{as } \lambda \to \infty. \tag{4.32}$$

We also find from (4.31) that $\mathrm{d}\phi/\mathrm{d}\xi = \sqrt{2}$ at $\xi = 0$ and deduce that

$$A \sim \sqrt{2\lambda} \quad \text{as } \lambda \to \infty. \tag{4.33}$$

The approximations (4.32) and (4.33) are shown as dashed curves in figures 7 and 8.

When we substitute (4.33) into (4.19) we find that $H(0) \sim B_0 \left(\delta \sqrt{2\lambda} \right)^{-1/7}$ as $\lambda \to \infty$. This implies that the film thickness at the origin decreases towards zero as the length of the beam increases, which seems physically implausible. This result is explained in the following section by a more careful examination of the combined asymptotic limits $\lambda \to \infty$ and $\delta \to 0$.

4.6. *New distinguished limit*

The analysis above demonstrates that, as the beam becomes longer, an increasing proportion of it is approximately vertical. Equation (4.29) shows how the region over which the deflection adjusts from $\phi = 0$ to $\phi \approx \pi/2$ becomes smaller as λ increases, with $S \sim \lambda^{-1/2}$. On the other hand, the width of the boundary layer over which the film thickness h adjusts is given by (4.14) as $S \sim \delta^{3/7} A^{-4/7} \sim \delta^{3/7} \lambda^{-2/7}$ as $\lambda \to \infty$. A new distinguished limit emerges in which these inner regions overlap when

$$\Delta = \delta \sqrt{\lambda} = \frac{3\rho v q L}{B} = O(1). \tag{4.34}$$

In this limit, the scaled film thickness $Y(\xi) = H(S)$ in the inner region satisfies

$$Y^3 \left(\Delta \cos\phi \frac{\mathrm{d}Y}{\mathrm{d}\xi} - \sin\phi \right) = -1, \tag{4.35}$$

subject to the matching condition $Y \to 1$ as $\xi \to \infty$, while the deflection angle ϕ is still given by (4.31).

This problem may be helpfully reformulated as

$$\Delta \frac{\mathrm{d}Y}{\mathrm{d}w} = \sec w + \operatorname{cosec} w \operatorname{cosec}(2w) \frac{1 - Y^3}{Y^3}, \tag{4.36}$$

where $w = \pi/4 - \phi/2$. For each value of Δ, this is easily solved numerically subject to the initial condition

$$Y \sim 1 + \frac{2w^2}{3} - \frac{8\Delta w^3}{9} + \frac{2\left(3 + 8\Delta^2\right) w^4}{9} + \cdots \quad \text{as } w \to 0. \tag{4.37}$$

Some numerical results for the film height $Y(\xi) = H(S)$ obtained by following this procedure are plotted in figure 10. For each value of Δ, we see that Y is a monotonically decreasing function of distance ξ from the origin, tending to 1 as $\xi \to \infty$. The film thickness at the origin $Y_0 = Y|_{w=\pi/4}$ is a decreasing function of Δ, as shown in figure 11. Here we plot the difference between the film thickness Y_0 at the origin and the thickness $H = 1$ in the outer region. This difference tends to zero as $\Delta \to \infty$ and the boundary layer at the origin shrinks to zero.

If we perform the scalings

$$\xi = 2^{-2/7} \Delta^{3/7} \hat{z}, \quad Y = 2^{-1/14} \Delta^{-1/7} \hat{h}, \tag{4.38}$$

before taking the limit $\Delta \to 0$, then (4.35) reduces to the previously solved problem (4.18). It is readily verified that (4.38) is consistent with the rescaling (4.14) when $A \sim (2\lambda)^{1/2}$. This allows us to read off the asymptotic behaviour

$$Y_0 \sim \frac{B_0}{2^{1/14} \Delta^{1/7}} \quad \text{as } \Delta \to 0, \tag{4.39}$$

as indicated by a dashed curve in figure 11.

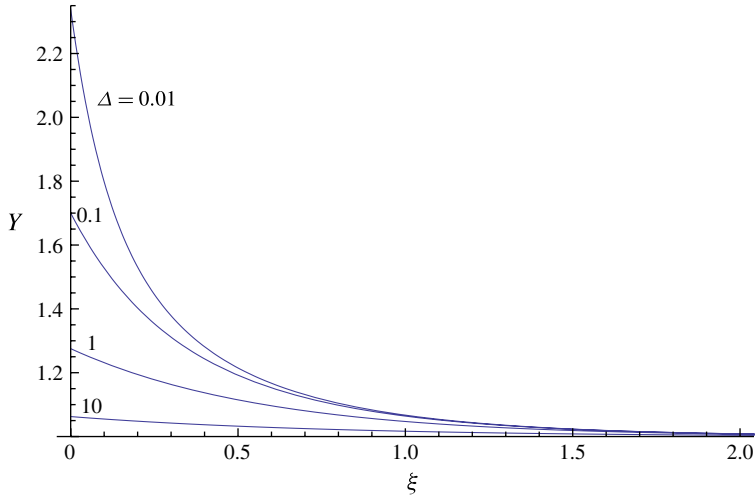FIGURE 10. (Colour online) The film thickness $Y(\xi)$ satisfying the inner (4.35) and $Y \to 1$ as $\xi \to \infty$, with $\Delta \in \{0.01, 0.1, 1, 10\}$.
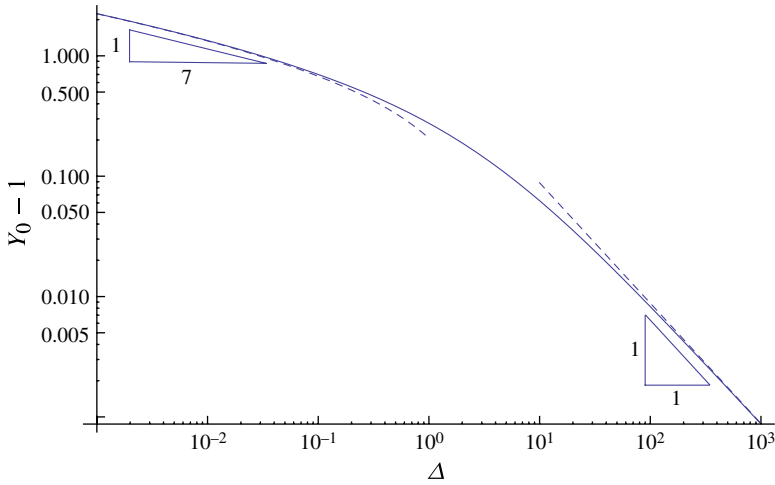

FIGURE 11. (Colour online) The excess film thickness at the origin, $Y_0 - 1$, plotted versus $\Delta = \delta\sqrt{\lambda}$ using logarithmic axes. The dashed curves show the asymptotic limits (4.39) as $\Delta \to 0$ and (4.41) as $\Delta \to \infty$.

On the other hand, we observe that $Y \sim 1$ when $\Delta \gg 1$, and we find that

$$Y \sim 1 + \frac{1}{\Delta} \log\left(\frac{1 + \tan(w/2)}{1 - \tan(w/2)}\right) = 1 + \frac{1}{\Delta} \log\left(\frac{1 + \left(\sqrt{2} - 1\right) e^{-\xi}}{1 - \left(\sqrt{2} - 1\right) e^{-\xi}}\right) \quad (4.40)$$

as $\Delta \to \infty$. Hence, we obtain the asymptotic behaviour

$$Y_0 \sim 1 + \frac{\log\left(1 + \sqrt{2}\right)}{\Delta} \quad \text{as } \Delta \to \infty, \tag{4.41}$$

which is also plotted in figure 11 using a dashed curve. Hence, when the beam becomes extremely long and flexible, the film thickness ultimately becomes completely uniform and $H(0) \to 1$.

5. Summary

Now we collect all of the asymptotic predictions obtained above and compare them with numerical solutions of the complete model with small but finite values of ε. It is helpful to pose the steady governing equations (4.2) as the first-order system

$$\frac{dH}{d\phi} = \frac{H^3 \sin \phi - 1}{\varepsilon^{16/9} H^3 \kappa \cos \phi}, \tag{5.1a}$$

$$\frac{d\mathscr{T}}{d\phi} = -\mathscr{N} - \frac{1}{H^2 \kappa}, \tag{5.1b}$$

$$\frac{d\mathscr{N}}{d\phi} = \mathscr{T} + \frac{H \cos \phi}{\kappa}, \tag{5.1c}$$

$$\frac{d\kappa}{d\phi} = \frac{\mathscr{N}}{\kappa}, \tag{5.1d}$$

$$\frac{d\tilde{S}}{d\phi} = -\frac{1}{\kappa}, \tag{5.1e}$$

where $\tilde{S} = \lambda - S$ and again $\kappa = d\phi/dS$ is the curvature. We shoot from $\phi = \Phi$, where $H = \mathscr{T} = \mathscr{N} = \kappa = \tilde{S} = 0$. The singularity is handled by using local expansions for the dependent variables, given in Appendix. We can then read off the values of $\lambda = \tilde{S}(0)$ and $H_0 = H(0)$ corresponding to each choice of ε and Φ.

In plotting our numerical results, we characterize the beam deflection by the angle Φ and the film thickness by the dimensionless variable

$$h_0 = \varepsilon^{1/3} H_0 = \frac{h_0^*}{\varepsilon a} = \left(\frac{\rho g^5}{81 B v^4 q^4}\right)^{1/16} h_0^*, \tag{5.2}$$

where we recall the notation h^* for the dimensional film thickness. The problem statement (5.1) makes it clear that h_0 and Φ depend on two independent dimensionless parameters, which we choose to be

$$\ell = \frac{L}{a} = \left(\frac{\rho g}{B}\right)^{1/4} L, \tag{5.3a}$$

$$\varepsilon = \left(\frac{3 v q}{g a^3}\right)^{1/4} = \left(\frac{81 v^4 q^4 \rho^3}{g B^3}\right)^{1/16}, \tag{5.3b}$$

characterizing the normalized beam length and the aspect ratio of the liquid film, respectively. In figures 12 and 13, we plot numerical results for the dimensionless film thickness h_0 at the origin and the beam deflection angle Φ, respectively, versus the dimensionless beam length ℓ, for two fixed values of $\varepsilon = 0.1$ and $\varepsilon = 0.01$.
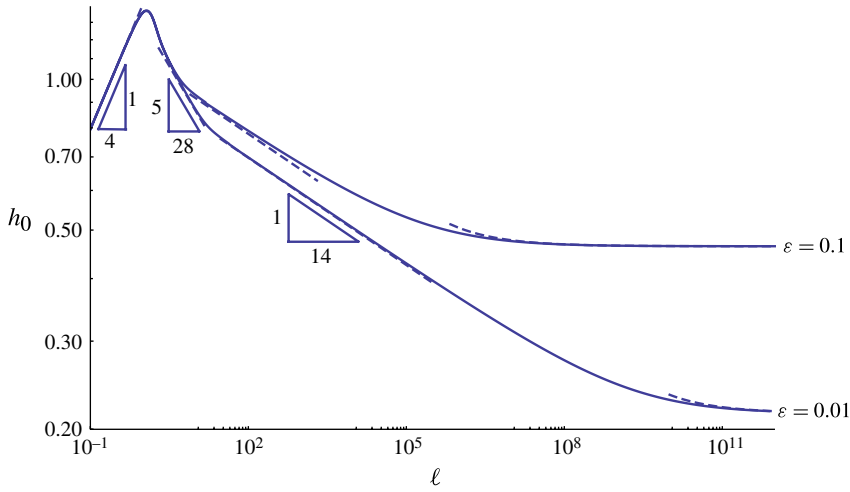
FIGURE 12. (Colour online) Dimensionless film thickness h_0 at the origin plotted versus dimensionless beam length ℓ using logarithmic axes, with $\varepsilon = 0.01$ and $\varepsilon = 0.1$. The dashed curves show the asymptotic approximations (5.4).

FIGURE 13. (Colour online) Beam deflection angle Φ plotted versus dimensionless beam length ℓ using logarithmic axes, with $\varepsilon = 0.01$ and $\varepsilon = 0.1$.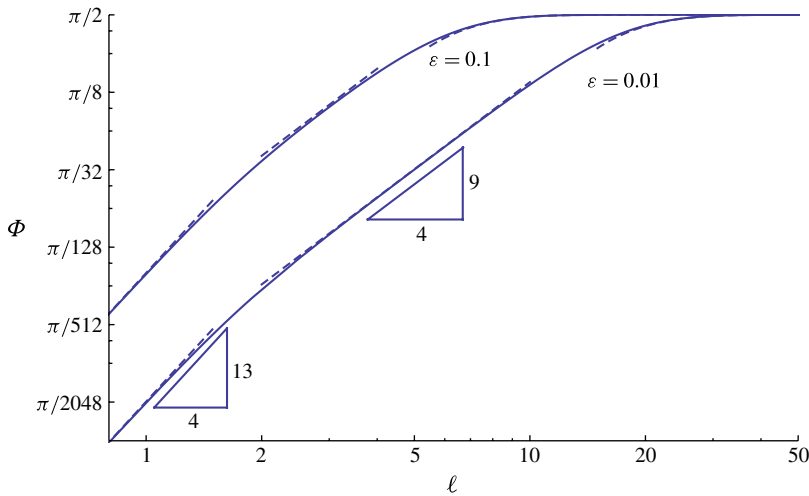 The dashed curves show the asymptotic approximations (5.5). (The tick marks on the vertical axis are at $\Phi = n\pi/2^{2m+1}$, where $n \in \{2, 3, 4\}$ and $m \in \{1, 2, 3, 4, 5, 6\}$.)

The small-deflection model analysed in §3 gives leading-order approximations of the form $h_0 = h_0(\ell)$ and $\Phi = \varepsilon\Psi(\ell)$ when $\ell = O(1)$. The large-deflection model from §4 is valid when $\ell = O\left(\varepsilon^{-4/9}\right)$ and gives us the solution in the form $h_0 = \varepsilon^{1/3}H_0\left(\varepsilon^{4/9}\ell\right)$ and $\Phi = \Phi\left(\varepsilon^{4/9}\ell\right)$. This approximation for Φ persists for arbitrarily large values of ℓ, but a different approximation for h_0 is found in §4.6 when $\ell = O\left(\varepsilon^{-4}\right)$, namely $h_0 = \varepsilon^{1/3}Y_0\left(\varepsilon^2\ell^{1/2}\right)$.

In §§ 3–4 we have verified that the solutions match in intermediate asymptotic regimes, and, for $\varepsilon \ll 1$, we can infer the following simplified approximations:

$$
h_0 \sim \begin{cases} \sqrt{2}\,\ell^{1/4}, & \ell \ll 1, \\ 1.30499\,\ell^{-5/28}, & 1 \ll \ell \ll \varepsilon^{-4/9}, \\ 1.20648\,\varepsilon^{1/21}\ell^{-1/14}, & \varepsilon^{-4/9} \ll \ell \ll \varepsilon^{-4}, \\ \varepsilon^{1/3} + \log(1+\sqrt{2})\varepsilon^{-5/3}\ell^{-1/2}, & \ell \gg \varepsilon^{-4}, \end{cases} \tag{5.4}
$$

and

$$
\Phi \sim \begin{cases} \dfrac{64\sqrt{2}}{585}\,\varepsilon\,\ell^{13/4}, & \ell \ll 1, \\ 0.26483\,\varepsilon\,\ell^{9/4}, & 1 \ll \ell \ll \varepsilon^{-4/9}, \\ \dfrac{\pi}{2} - \dfrac{8\left(\sqrt{2}-1\right)\sqrt{\pi}}{3^{1/6}\Gamma(2/3)}\,\varepsilon^{1/9}\,\ell^{1/4}\exp\left(-\dfrac{2}{3}\,\varepsilon^{2/3}\ell^{3/2}\right), & \ell \gg \varepsilon^{-4/9}. \end{cases} \tag{5.5}
$$

The dashed curves in figures 12 and 13 show how these estimates are manifested as ℓ varies. As expected, the different intermediate asymptotic regimes are more clearly distinguished when ε is decreased.

6. Conclusions

In this paper, we have studied a model problem in which the flow of a thin liquid film and the deformation of an elastic substrate are intrinsically coupled. The substrate is a flexible beam whose weight is assumed to be negligible, so that its deflection is solely due to the liquid film on its upper surface. On the other hand, the principal driving force for the liquid film is the tangential component of gravity created by the deflection of the substrate. This strong mutual coupling gives rise to a fascinating range of possible behaviours as the dimensionless liquid flux and beam length are varied. For example, for a fixed liquid flux, we find that the thickness of the resulting film first increases and then decreases as the length of the beam increases. With the benefit of hindsight, this is a clear consequence of the fluid–elastic coupling: a longer beam suffers a greater deflection which enhances the gravitational forcing experienced by the fluid and therefore promotes flow away from the applied source. Thus, the deflection of a leaf in the rain facilitates the removal of water from its surface.

Our mathematical model is based on several simplifications whose validity is open to question. For example, we have assumed that lubrication theory is valid and that the effect of the surface tension γ is negligible throughout. On the face of it, these assumptions are valid provided the slenderness parameter ε and the reduced Reynolds number $\mathrm{Re} = \varepsilon q/3\nu$ are sufficiently small, and the Bond number $\mathrm{Bo} = \rho g a^2/\gamma$ is sufficiently large. For example, the data given by Gibson, Ashby & Easterling (1988) imply that the bending stiffness of a leaf is in the range 0.1–1 N m and, hence, that the characteristic bending length scale a is around 6–10 cm (interestingly, this is also a reasonable length scale for a typical leaf). For a substrate with similar elastic properties, ε and Re are small for all values of the flux such that $q \ll 1$ cm^2 s^{-1}, and the Bond number is at least 500.

However, the potential effects of both two-dimensionality and capillarity may be amplified when there are boundary layers in the solution. In particular, there will certainly be a neighbourhood of the free end where the approximations made herein

fail. Our simplified boundary condition of vanishing film thickness as the liquid falls from the end of the beam appears to be a reasonable matching condition at least while the deflection angle remains small. For larger deflections, although this condition is no longer physically realistic, it has negligible influence on the outer solution.

In practice, rather than immediately detaching from the free end of the beam, the liquid film would form a viscous jet that accelerates away from the beam under gravity. By dimensional analysis, one may estimate that this jet exerts a tension on the end of the beam of order $\rho q (\nu g)^{1/3}$. Our zero-stress boundary conditions applied at the free end of the beam are valid provided this tension is much smaller than the scaling (2.8b) used for the tension in the beam. The relevant dimensional parameter is found to be $q\nu^{1/3}/\varepsilon^2 a^2 g^{2/3} = (\varepsilon \mathrm{Re}/3)^{1/3} \ll 1$, so the influence of the falling jet is indeed negligible at leading order whenever lubrication theory is valid for the film on the beam. (We are grateful to an anonymous referee for suggesting this analysis.)

The time-dependent version of this problem promises intriguing dynamics, with the various asymptotic regimes discovered in this paper being encountered in turn as the film spreads along the substrate, and we intend to explore this in future work. We note also that the simple physical situation considered in this paper appears relatively straightforward to study experimentally; indeed we are currently pursuing experimental validation of our results. It would also be interesting to generalize the geometrical set-up, for example by considering a naturally curved substrate or by varying the angle at which it is clamped.

Acknowledgements

Appendix. Local expansions near the end of the beam

To solve the system (5.1) numerically, we use the following local expansions:

$$H \sim \frac{8}{\sin^{1/3}\Phi}\,\mu\left\{1 - 71\mu^3 + \frac{2699058}{1045}\,\mu^6 + \cdots\right\}, \tag{A1a}$$

$$\mathscr{T} \sim \frac{32\varepsilon^{16/9}}{\sin^{2/3}\Phi}\,\mu^2\left\{1 + \frac{314}{5}\,\mu^3 + \frac{3175401}{1045}\,\mu^6 + \cdots\right\}, \tag{A1b}$$

$$\mathscr{N} \sim -\frac{32768\varepsilon^{16/9}\cos^2\Phi}{5\sin^{5/3}\Phi}\,\mu^5\left\{1 - 35\mu^3 + \frac{150588}{209}\,\mu^6 + \cdots\right\}, \tag{A1c}$$

$$\kappa \sim \frac{134217728\varepsilon^{32/9}}{45\tan^3\Phi}\,\mu^9\left\{1 - 15\mu^3 + \frac{32958}{209}\,\mu^6 + \cdots\right\}, \tag{A1d}$$

$$\tilde{S} \sim \frac{1024\varepsilon^{16/9}\cos\Phi}{\sin^{4/3}\Phi}\,\mu^4\left\{1 + \frac{60}{7}\,\mu^3 + \frac{28134}{1045}\,\mu^6 + \cdots\right\} \tag{A1e}$$

where

$$\phi = \Phi - \frac{549755813888\varepsilon^{16/3}\cos^4\Phi}{585\sin^{13/3}\Phi}\,\mu^{13} \tag{A1f}$$

and $0 < \mu \ll 1$. As $\Phi \to 0$, we require $\mu \ll (\Phi/\varepsilon)^{16/39}$.

As $\Phi \to \pi/2$, the boundary layer in H at $\phi = \Phi$ makes the problem very stiff numerically, and we instead apply the matching condition $H = \mathrm{cosec}^{1/3}\Phi$ when $\phi = \Phi$. In this case the appropriate local expansions are

$$H \sim \mathrm{cosec}^{1/3}\Phi + \frac{3^{1/3}\sin^{1/9}\Phi}{2^{5/3}\varepsilon^{16/9}\cos^{1/3}\Phi}(\Phi - \phi)^{4/3} + \cdots, \tag{A 2a}$$

$$\mathscr{T} \sim \frac{6^{1/3}\sin^{7/9}\Phi}{\cos^{1/3}\Phi}(\Phi - \phi)^{1/3} - \frac{49 + 41\cos(2\Phi)}{20 \cdot 6^{2/3}\cos^{4/3}\Phi\sin^{2/9}\Phi}(\Phi - \phi)^{4/3} + \cdots, \tag{A 2b}$$

$$\mathscr{N} \sim -\frac{6^{1/3}\cos^{2/3}\Phi}{\sin^{2/9}\Phi}(\Phi - \phi)^{1/3} - \frac{14 \cdot 2^{1/3}\sin^{7/9}\Phi}{5 \cdot 3^{2/3}\cos^{1/3}\Phi}(\Phi - \phi)^{4/3} + \cdots, \tag{A 2c}$$

$$\kappa \sim \frac{3^{2/3}\cos^{1/3}\Phi}{2^{1/3}\sin^{1/9}\Phi}(\Phi - \phi)^{2/3} + \frac{2^{5/3}\sin^{8/9}\Phi}{5 \cdot 3^{1/3}\cos^{2/3}\Phi}(\Phi - \phi)^{5/3} + \cdots, \tag{A 2d}$$

$$\tilde{S} \sim \frac{6^{1/3}\sin^{1/9}\Phi}{\cos^{1/3}\Phi}(\Phi - \phi)^{1/3} - \frac{2^{1/3}\sin^{16/9}\Phi}{5 \cdot 3^{2/3}\cos^{4/3}\Phi}(\Phi - \phi)^{4/3} + \cdots \tag{A 2e}$$

as $\phi \to \Phi$.

REFERENCES

BOUSSINESQ, J. 1904 Recherches théoriques sur l'écoulement des nappes d'eau infiltrées dans le sol et sur le débit des sources. *J. Math. Pure Appl.* **10**, 5–78.

CRASTER, R. V. & MATAR, O. K. 2009 Dynamics and stability of thin liquid films. *Rev. Mod. Phys.* **81** (3), 1131–1198.

DUFFY, B. R. & WILSON, S. K. 1999 Thin-film and curtain flows on the outside of a rotating horizontal cylinder. *J. Fluid Mech.* **394**, 29–49.

GIBSON, L. J., ASHBY, M. F. & EASTERLING, K. E. 1988 Structure and mechanics of the iris leaf. *J. Mater. Sci.* **23** (9), 3041–3048.

HALPERN, D. & GROTBERG, J. B. 1992 Fluid-elastic instabilities of liquid-lined flexible tubes. *J. Fluid Mech.* **244**, 615–632.

HEIL, M. & WHITE, J. P. 2002 Airway closure: surface-tension-driven non-axisymmetric instabilities of liquid-lined elastic rings. *J. Fluid Mech.* **462**, 79–109.

HOWELL, P. D. 2003 Surface-tension-driven flow on a moving curved surface. *J. Eng. Math.* **45** (3–4), 283–308.

HUPPERT, H. E. 1982a Flow and instability of a viscous current down a slope. *Nature* **300** (5891), 427–429.

HUPPERT, H. E. 1982b The propagation of two-dimensional and axisymmetric viscous gravity currents over a rigid horizontal surface. *J. Fluid Mech.* **121**, 43–58.

JENSEN, O. E. 1997 The thin liquid lining of a weakly curved cylindrical tube. *J. Fluid Mech.* **331**, 373–403.

MATAR, O. K., CRASTER, R. V. & KUMAR, S. 2007 Falling films on flexible inclines. *Phys. Rev. E* **76** (5), 056301.

MATAR, O. K. & KUMAR, S. 2007 Dynamics and stability of flow down a flexible incline. *J. Eng. Math.* **57** (2), 145–158.

MYERS, T. G., CHARPIN, J. P. F. & CHAPMAN, S. J. 2002 The flow and solidification of a thin fluid film on an arbitrary three-dimensional surface. *Phys. Fluids* **14** (8), 2788–2803.

ORON, A., DAVIS, S. H. & BANKOFF, S. G. 1997 Long-scale evolution of thin liquid films. *Rev. Mod. Phys.* **69** (3), 931–980.

ROY, R. V., ROBERTS, A. J. & SIMPSON, M. E. 2002 A lubrication model of coating flows over a curved substrate in space. *J. Fluid Mech.* **454**, 235–261.

RUPP, D. E. & SELKER, J. S. 2005 Drainage of a horizontal Boussinesq aquifer with a power law hydraulic conductivity profile. *Water Resour. Res.* **41** (11), W11422.

TAKAGI, D. & HUPPERT, H. E. 2010 Flow and instability of thin films on a cylinder and sphere. *J. Fluid Mech.* **647**, 221–238.

ZHENG, Z., SOH, B., HUPPERT, H. E. & STONE, H. A. 2013 Fluid drainage from the edge of a porous reservoir. *J. Fluid Mech.* **718**, 558–568.